RNA (2000), *6*:409–421. Cambridge University Press. Printed in the USA.

Contribution of the intercalated adenosine at the helical junction to the stability of the *gag-pro* frameshifting pseudoknot from mouse mammary tumor virus

CARLA A. THEIMER and DAVID P. GIEDROC

Department of Biochemistry and Biophysics, Center for Macromolecular Design, Texas A&M University, College Station, Texas 77843-2128, USA

ABSTRACT

The mouse mammary tumor virus (MMTV) *gag-pro* frameshifting pseudoknot is an H-type RNA pseudoknot that contains an unpaired adenosine (A14) at the junction of the two helical stems required for efficient frameshifting activity. The thermodynamics of folding of the MMTV vpk pseudoknot have been compared with a structurally homologous mutant RNA containing a G•U to G-C substitution at the helical junction (U13C RNA), and an A14 deletion mutation in that context (U13CΔA14 RNA). Dual wavelength optical melting and differential scanning calorimetry reveal that the unpaired adenosine contributes 0.7 (±0.2) kcal mol^{-1} at low salt and 1.4 (±0.2) kcal mol^{-1} to the stability ($\Delta G°_{37}$) at 1 M NaCl. This stability increment derives from a favorable enthalpy contribution to the stability $\Delta\Delta H = 6.6$ (±2.1) kcal mol^{-1} with $\Delta\Delta G°_{37}$ comparable to that predicted for the stacking of a dangling 3′ unpaired adenosine on a G-C or G•U base pair. Group 1A monovalent ions, NH_4^+, Mg^{2+}, and $Co(NH_3)_6^{3+}$ ions stabilize the A14 and ΔA14 pseudoknots to largely identical extents, revealing that the observed differences in stability in these molecules do not derive from a differential or specific accumulation of ions in the A14 versus ΔA14 pseudoknots. Knowledge of this free energy contribution may facilitate the prediction of RNA pseudoknot formation from primary nucleotide sequence (Gultyaev et al., 1999, *RNA 5*:609–617).

Keywords: frameshifting; MMTV; nucleic acid stability; RNA pseudoknot; thermodynamics

INTRODUCTION

The structures of complex RNAs show that regulatory, structural, and catalytic RNAs adopt well-defined globular or tertiary structures where secondary structural units (helices) pack against one another (see Strobel and Doudna, 1997, for a review). These higher-order structures are stabilized by helix–helix stacking interactions in the formation of 2, 3, and 4-helix junctions and by helix–single-stranded loop and loop–loop interactions, some of which are stabilized or mediated by divalent cations. An RNA pseudoknot constitutes one of the simplest RNA folding motifs containing a two-helix junction. Pseudoknots play fundamental roles in structurally organizing complex RNAs, and in translational regulation where they modulate ribosome loading and stimulate translational recoding or frameshifting within the coding regions of mRNAs (Atkins & Gesteland, 1999). For example, hairpin-type (H-type) RNA pseudoknots stimulate ribosomal frameshifting when they are positioned 3′ to an mRNA slippery sequence (Chamorro et al., 1992), although the precise mechanism remains undefined.

An H-type pseudoknot consists of an RNA hairpin that forms the 5′ helical stem of the pseudoknot (stem 1) and the first loop of the pseudoknot (loop 1). This is followed by a single-stranded region that forms the second loop of the pseudoknot (loop 2) and a region complementary to part of the hairpin loop sequence, which forms the second helical stem of the pseudoknot (stem 2) (Fig. 1). The helical stems can be coaxially stacked and nearly colinear (Du & Hoffman, 1997; Hol-

Reprint requests to: David P. Giedroc, Department of Biochemistry and Biophysics, Center for Macromolecular Design, Texas A&M University, College Station, Texas 77843-2128, USA; e-mail: giedroc@tamu.edu.

Abbreviations: BWYV: beet western yellows virus; EDTA: ethylenediamine-tetraacetic acid; FIV: feline immunodeficiency virus; IBV: infectious bronchitis virus; mIAP: mouse intracisternal A-type particle; MMTV: mouse mammary tumor virus; MOPS: 3-[*N*-morpholino]propanesulfonic acid; PAGE: polyacrylamide gel electrophoresis; SRV-1: simian retrovirus-1.

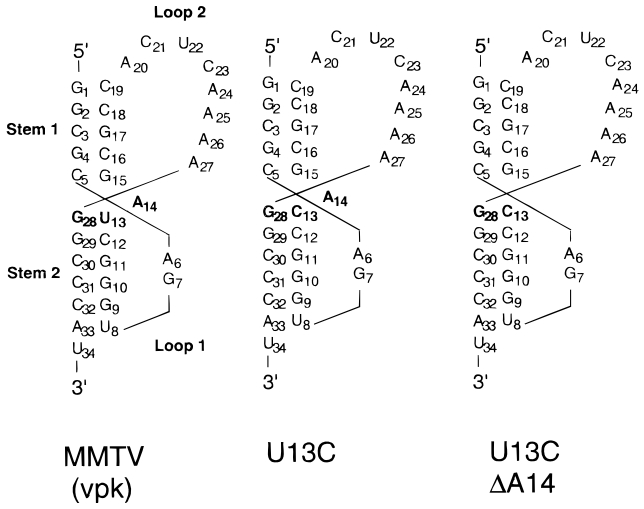

FIGURE 1. The secondary structural representations of the MMTV pseudoknots vpk, U13C, and U13CΔA14 characterized in this study.

land et al., 1999) or strongly bent (Shen & Tinoco, 1995; Su et al., 1999).

The mouse mammary tumor virus (MMTV) *gag-pro* 1 frameshifting pseudoknot has been subjected to mutational analysis and structure probing (Chamorro et al., 1992; Chen et al., 1995) and the solution structure has been solved by NMR spectroscopy (Shen & Tinoco, 1995). Recently, a refined NMR solution structure of the MMTV pseudoknot was published with a larger number of loop-to-stem constraints for loop 1 because of NOEs with a coordinated $Co(NH_3)_6^{3+}$ ion (Gonzalez & Tinoco, 1999). Solution structures of frameshifting and nonframeshifting variants have also been determined (Chen et al., 1996; Kang et al., 1996; Kang & Tinoco, 1997). Frameshifting efficiency in these MMTV pseudoknot derivatives was found to correlate with a specific bent conformation where the helical junction was prevented from coaxially stacking by a single unpaired adenosine intercalated between the two stems. Further evidence for the importance of an unpaired nucleotide(s) at the helical junction comes from functional studies on pseudoknot chimeras formed between the infectious bronchitis virus (IBV)*1a-1b* and MMTV *gag-pro* pseudoknots (Liphardt et al., 1999), in which high efficiency frameshifting RNAs were found to contain an unpaired adenosine at the junction of two six-base pair stems in addition to other favorable and functionally important interactions between the 3′ end of loop 2 and the base pairs at the bottom of stem 1 proximal to the junction. The extent to which these structural determinants characterize other *gag-pol* pseudoknots, like simian retrovirus-1 (SRV-1) and feline immunodeficiency virus (FIV) is not known, although a weakly base-paired or unpaired junction may characterize these systems as well (Morikawa & Bishop, 1992; Chen et al., 1995; Du et al., 1997; Sung & Kang, 1998). Folding studies on variants of the *gag-pro* frameshifting pseudoknot from mouse intracisternal A-type particles (mIAP), reveal that this RNA has a weakly paired or nonbase-paired junction similar to that of SRV-1, because the small destabilization observed upon deletion of the helical junction adenosine [$\Delta\Delta G^\circ_{37} \approx 1$ kcal mol^{-1}] could not be attributed to the loss of an A-U base pair (Theimer & Giedroc, 1999).

Studies on the thermodynamics of folding of frameshifting versus nonframeshifting pseudoknots are required to determine the origin of the stability of active versus inactive conformations as well as the degree to which active conformers are stabilized relative to nonframeshifting or partially folded molecules. In this study, we have examined the thermodynamic and ion-binding properties of frameshifting and nonframeshifting variants of the MMTV *gag-pro* pseudoknot and have determined the energetics and contribution that an unpaired adenosine at the helical junction makes to the global stability of this pseudoknot. This is an important issue since a single nucleotide bulge at the junction of two helical stems can strongly alter the stacking of the pseudoknot stems and, in turn, have unpredictable effects on the thermodynamic stability of the pseudoknot. Indeed, in all cases that we have studied, loop substitution or deletion mutations are never energetically silent, and can have significant effects on the energetics of folding and global stability (Theimer et al., 1998; Theimer & Giedroc, 1999). We show here that the unpaired "wedge" adenosine in the MMTV pseudoknot makes a stabilizing contribution of 1.4 ($\pm$ 0.2) kcal mol^{-1} at 1 M Na^+ (ΔG°_{37}) toward the stability of a bent versus linear pseudoknot, or a contribution comparable to a dangling 3′ single-stranded stack on a helical stem (Turner et al., 1988). Knowledge of this free energy contribution may facilitate the prediction of RNA pseudoknot formation from primary structure.

RESULTS

Extensive structural and functional analyses of the MMTV pseudoknot have been reported not only for the wild-type sequence, but also on active and inactive mutant forms, making this an attractive system for thermodynamic studies (Chamorro et al., 1992; Chen et al., 1995, 1996; Shen & Tinoco, 1995; Kang et al., 1996; Kang & Tinoco, 1997). This includes an investigation of the extent of stabilization of the MMTV vpk pseudoknot by mono- and divalent ions (Gonzalez & Tinoco, 1999). This work focuses on three MMTV *gag-pro* shift site-derived RNAs (Fig. 1). The wild-type RNA is a variant MMTV pseudoknot, termed vpk, whose structure has been solved by NMR (Shen & Tinoco, 1995; Gonzalaz & Tinoco, 1999). We also studied two RNAs with mutations at the helical junction, one of which, U13C, has the same bent structure and equivalent frameshifting efficiency as vpk, whereas the other,

U13CΔA14, has coaxially stacked helices and is not functional in frameshifting (Fig. 1; Chen et al., 1995, 1996). The junction adenosine (A14) deletion was studied in the context of the U13C base substitution because, in the vpk context (i.e., U13), deletion of A14 eliminates pseudoknot formation by stabilizing an alternate hairpin structure (Chen et al., 1995). The only difference in sequence between the active U13C and the inactive U13CΔA14 pseudoknots is the presence or absence of an unpaired, intercalated adenosine at the junction.

Thermal unfolding of the MMTV pseudoknots

Thermal denaturation of the pseudoknots shown in Figure 1 was monitored using dual-wavelength optical melting profiles and differential scanning calorimetry. Optical melting profiles acquired at 260 and 280 nm (plotted as (∂A/∂T vs. T) and differential scanning calorimetry profiles for the MMTV-derived pseudoknots in the absence of exogenously added Mg^{2+} are shown in Figure 2 with the thermodynamic parameters compiled in Table 1. The optical melting profile of MMTV vpk exhibits hy-

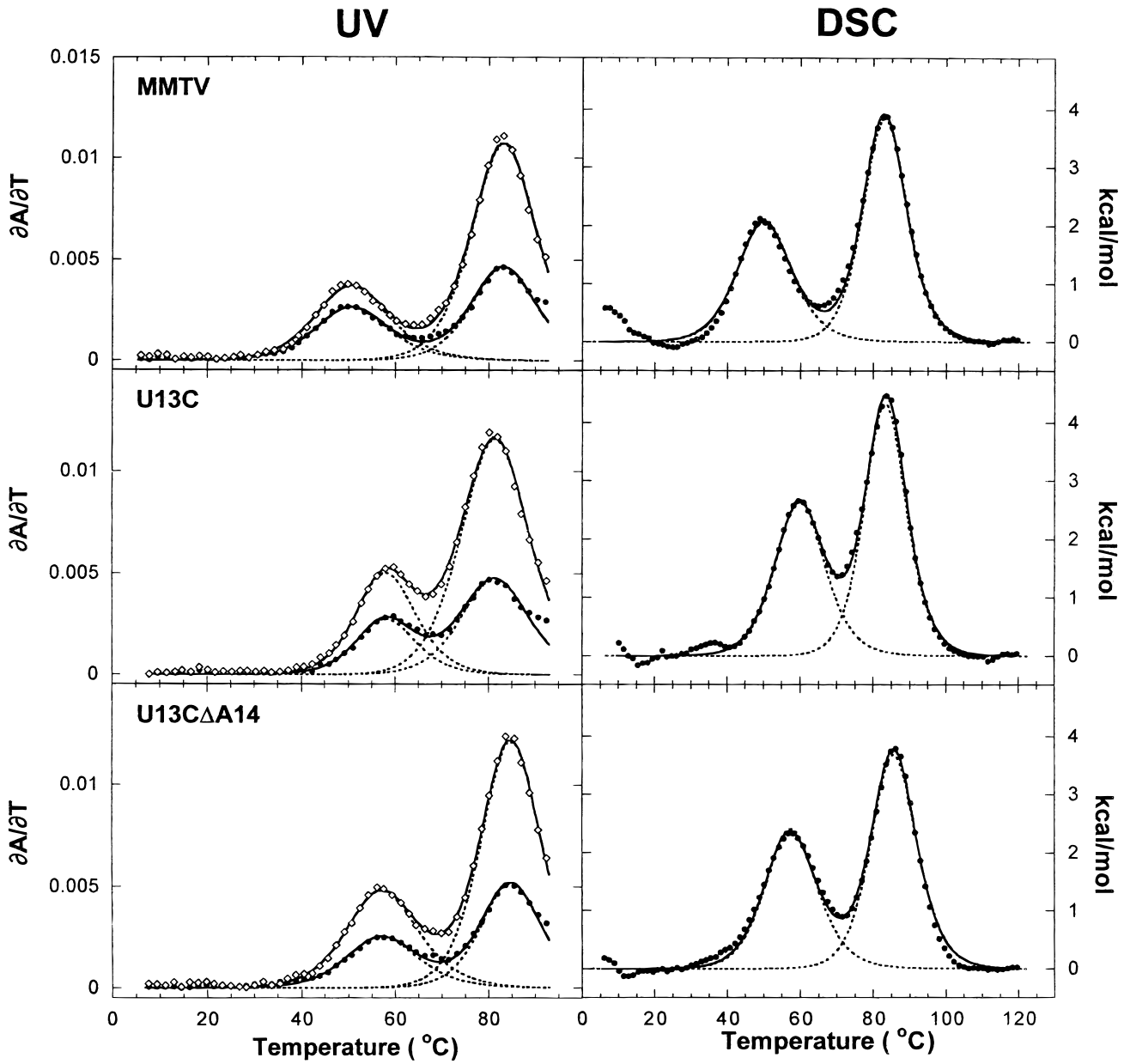

FIGURE 2. Optical and calorimetric melting profiles for the MMTV pseudoknots in the absence of exogenously added Mg^{2+} at 50 mM KCl. Optical melting profiles are shown on the left, with DSC profiles shown on the right. The composite fit (solid line) is superimposed on the calorimetry data (•). Optical data is represented by black (•) and gray-scale (◇) corresponding to ∂A/∂T monitored at 260 and 280 nm, respectively, with the fits represented as solid lines. Individual transitions are represented by dashed lines.

TABLE 1. Thermodynamic parameters derived for the unfolding of MMTV-derived pseudoknots.[a]

	Transition 1 pseudoknot → hairpin			Transition 2 hairpin → unfolded						
RNA	$\Delta H_{predict}$	ΔH_{vH}	t_m	$\Delta H_{predict}$	ΔH_{vH}	t_m	ΔH_{vH}^{total}	ΔH_{cal}	$\Delta G°_{37predict}$	$\Delta G°_{37}$
50 mM KCl										
MMTV vpk	—	41.5 (41.7)	50.2 (48.0)	—	62.7 (54.5)	83.0 (80.5)	104	107	—	9.8
U13C	—	48.1 (51.2)	60.0 (58.1)	—	66.7 (51.2)	85.7 (81.6)	115	115	—	12.4
U13CΔA14	—	44.7 (42.5)	58.3 (57.4)	—	64.6 (58.9)	86.0 (84.9)	109	108	—	11.7
0.5 mM Mg^{2+}										
MMTV vpk	—	42.4 (42.5)	61.7 (63.3)	—	65.6 (52.6)	89.7 (91.1)	108	105	—	12.7
U13C	—	48.6 (49.6)	72.5 (75.0)	—	70.0 (59.7)	90.8 (91.7)	119	120	—	15.3
U13CΔA14	—	46.7 (40.3)	72.4 (74.8)	—	66.4 (64.6)	92.2 (92.3)	113	112	—	14.8
1 M NaCl										
MMTV vpk	53.8	52.0 (40.6)	73.5 (72.9)	59.1	64.9 (64.6)	95.0 (94.8)	117	111	15.8	15.7
U13C	53.8	56.6 (55.8)	82.0 (79.9)	64.1	70.5 (66.4)	98.0 (95.5)	127	126	17.4	18.8
U13CΔA14	53.8	51.4 (41.0)	81.3 (81.4)	64.1	66.1 (70.0)	98.3 (99.0)	118	117	17.4	17.3

[a]Enthalpy and free energy are reported in kcal mol^{-1} and t_m is reported in °C. Thermodynamic parameters for DSC data were determined using the two-state model without a ΔCp contribution. Parameters derived from the optical melting profiles are shown in parenthesis for comparison with the DSC data.

perchromicity in two unfolding transitions, a lower intensity transition with ΔH and t_m of 42 kcal mol^{-1} and 48 °C, respectively, and a higher intensity transition at 80 °C with an enthalpy of 55 kcal mol^{-1} in the presence of 50 mM KCl. Each unfolding transition possesses significant hyperchromicity at 280 nm as expected for the high GC content of the two helical stems (Fresco et al., 1963). The DSC and optical data are in excellent agreement with one another except for the ΔH calculated for the unfolding of the hairpin intermediate (Table 1) which cannot be accurately determined from optical data, as they can only be collected to 95 °C (Fig. 2).

Turner rules compiled at 1 M NaCl calculated using the modified individual nearest-neighbor model (INN-HB) predict an enthalpy of 54 and 59 kcal mol^{-1} for the unfolding of helical stems 1 and 2, respectively, the latter including stacking of the 3′-terminal single-stranded uridine on the stem 2 helix, but not including any stabilization from helix–helix stacking at the helical junction or stacking of A14 on either helix (Turner et al., 1988; Xia et al., 1998; Mathews et al., 1999; Wyatt et al., 1990). The simplest interpretation of these melting profiles is that the two unfolding transitions correspond to the fully folded pseudoknot (PK) to hairpin (HP) intermediate and hairpin (HP) to unfolded (U) transitions, respectively, with no other significantly populated intermediates. The HP intermediate can either correspond to the partially folded stem 1 or stem 2 hairpin. Although it is reasonable to conclude that the first unfolding transition corresponds to a PK → S1 hairpin intermediate based on the perturbations in the hyperchromicity ratio of the first transition as a result of a G•U to G-C base-pair substitution in stem 2 (Fig. 2, below) as well as the close correspondence of the melting transition observed for a S1 hairpin RNA and the HP → U transition (data not shown), the actual assignment is immaterial to the conclusions reached regarding global or relative stability changes.

The U13C RNA optical and DSC melting profiles are very similar to that of the MMTV pseudoknot (Fig. 2). The PK → HP transition is stabilized significantly with an ≈8 kcal mol^{-1} and 10 °C increase in the ΔH and t_m, respectively, with a much smaller increase in the stability of the second transition (≈4 kcal mol^{-1} in ΔH and 3 °C in t_m; Table 1). On average, the U13C RNA is more stable than the MMTV vpk pseudoknot by 2.6 kcal mol^{-1} in free energy at 37 °C, totally consistent with the substitution of a terminal G•U base pair with a G-C base pair from secondary structure predictions (Xia et al., 1998; Table 1).

The U13CΔA14 deletion mutation could be stabilizing relative to the U13C RNA if the deletion allows coaxial stacking across the junction otherwise not present, neutral, or destabilizing if A14 in the wild-type context is involved in stacking of the helical stems or maintenance of a maximally stabilized junction conformation. In the absence of added Mg^{2+}, the U13CΔA14 RNA melting profile is qualitatively identical to U13C with small decreases in unfolding enthalpy determined for each transition (Table 1), indicating that the A14 nucleotide has a stabilizing effect and may potentially be involved in stacking. Although the experimental ΔH for the PK → HP transition is sensitive to solution conditions and is difficult to precisely measure, the difference in ΔH between the U13C and U13CΔA14 RNAs (ΔΔH) is largely insensitive to changes in solution conditions and was found to be 6.6 ± 2.1 kcal mol^{-1} for the PK → HP unfolding transition. Because the structural information for this molecule indicates that the two stems are coaxially stacked (Chen et al., 1996), this suggests that stacking of the unpaired adenosine between the helical stems in U13C is slightly more enthalpically stabilizing than coaxial stacking in this context.

Effects of multivalent ions on pseudoknot stability

The close approach of backbone phosphates at the helical junction in RNA pseudoknots can create a region high in negative electrostatic potential. This or nearby regions have been suggested as a possible location for association of divalent metal ions that bind with higher affinity than to duplex RNA (Puglisi et al., 1990; Gluick et al., 1997; Nixon & Giedroc, 1998). Therefore, mutations at the helical junction might significantly alter higher affinity divalent metal ion binding sites in otherwise similar RNAs. To examine this possibility in this system, the Mg^{2+} binding properties of the three MMTV RNAs were determined by examining the effect of Mg^{2+} on the melting profiles.

Optical and DSC melting profiles in the presence of 0.5 mM Mg^{2+} are shown in Figure 3 with thermodynamic parameters compiled in Table 1. All three RNAs show significant stabilization in the presence of 0.5 mM Mg^{2+}. The stabilization is of the same magnitude in all three cases such that the differences in free energy

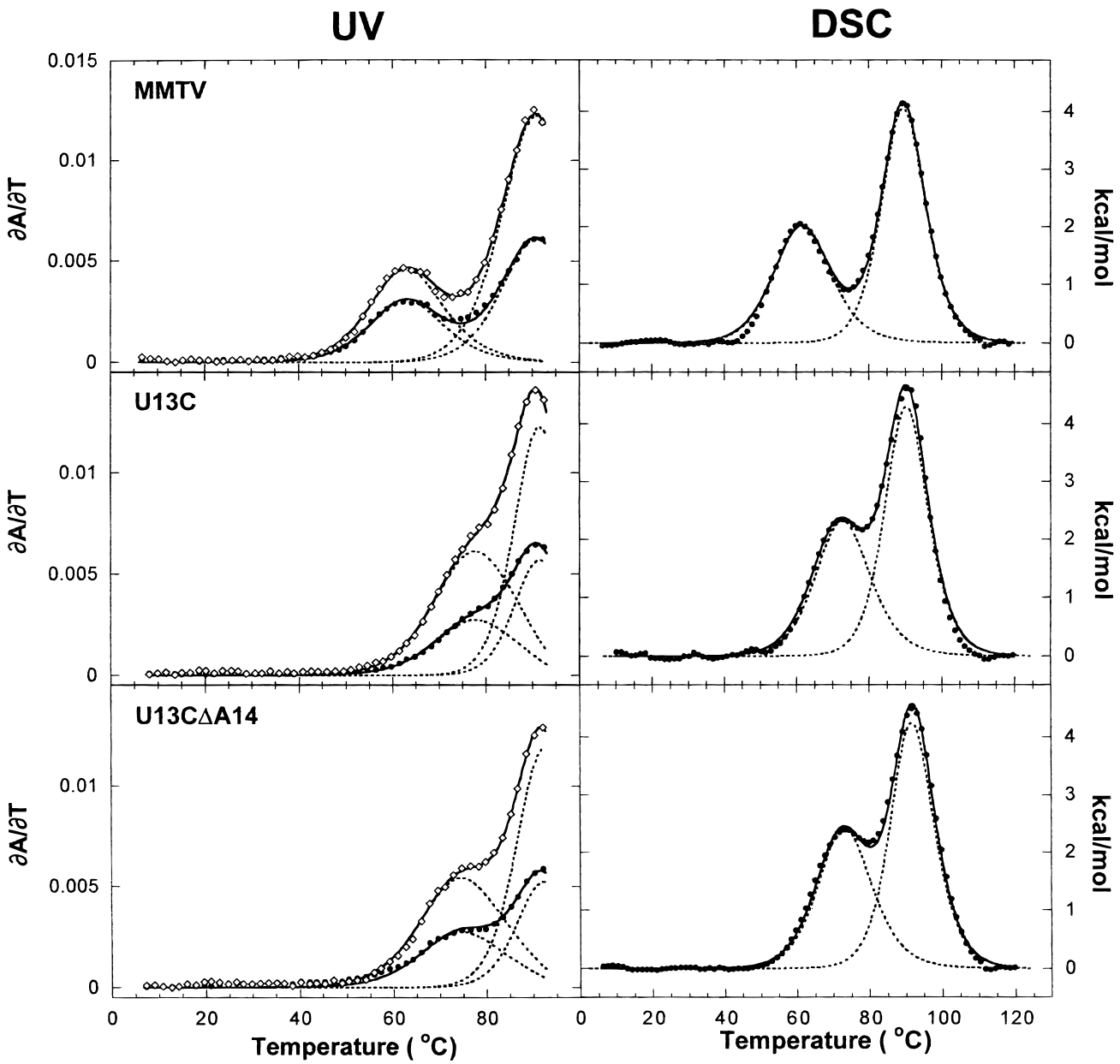

FIGURE 3. Optical and calorimetric melting profiles for the MMTV pseudoknots in the presence of 0.5 mM Mg^{2+} and 50 mM KCl. Optical melting profiles are shown on the left, with DSC profiles shown on the right. The composite fit (solid line) is superimposed on the calorimetry data (•). Optical data is represented by black (•) and gray-scale (◇) corresponding to ∂A/∂T monitored at 260 and 280 nm, respectively, with the fits represented as solid lines. Individual transitions are represented by dashed lines.

between the pseudoknots are roughly the same as those observed in the absence of Mg^{2+} (Table 1). The unfolding of the MMTV vpk pseudoknot was studied over a wide range of Mg^{2+} concentrations (50 μM–50 mM) in a background of 50 mM KCl with the data shown in Figure 4A in the form of $1/t_m$ versus log [Mg^{2+}] plots. Given the observed nonlinear dependence of $1/t_m$ on log [Mg^{2+}], these data were fit to a nonspecific binding model for divalent ions in which the folded and unfolded forms of the RNA participating in the transition have significant affinities for Mg^{2+} (Laing et al., 1994; Gluick et al., 1997; Nixon & Giedroc, 1998). The Mg^{2+} binding affinities for the folded (K_f) and unfolded (K_u) forms were found to be 2,100 ($\pm$150) M^{-1} and 600 ($\pm$50) M^{-1}, respectively, for the pseudoknot-to-hairpin transition and 1,600 ($\pm$300) M^{-1} and 800 ($\pm$200) M^{-1} for the hairpin-to-unfolded transition. The nonspecific model fits the data extremely well with a net total of $\approx$1.1 Mg^{2+} ions released upon unfolding the pseudoknot stem and $\approx$0.8 Mg^{2+} ions released upon unfolding the hairpin at 0.25 mM Mg^{2+} as shown in Figure 4B. As found previously, these data suggest that the fully folded pseudoknot sequesters slightly more ions bound with higher average affinities relative to a similarly sized RNA duplex, which are ultimately released upon unfolding (Nixon et al., 1999).

Investigation of the Mg^{2+}-dependence of the unfolding of the U13C and U13CΔA14 RNAs reveals that the apparent binding affinity for Mg^{2+} ions linked to the stabilization determined for these RNAs is similar to those observed for the MMTV vpk RNA, with approximately the same net release of Mg^{2+} ions observed upon unfolding within experimental error (Table 2). The magnitudes of K_f and K_u, which represent the average affinities of each form of the RNAs for Mg^{2+}, are reasonable for nonspecific binding in a background of

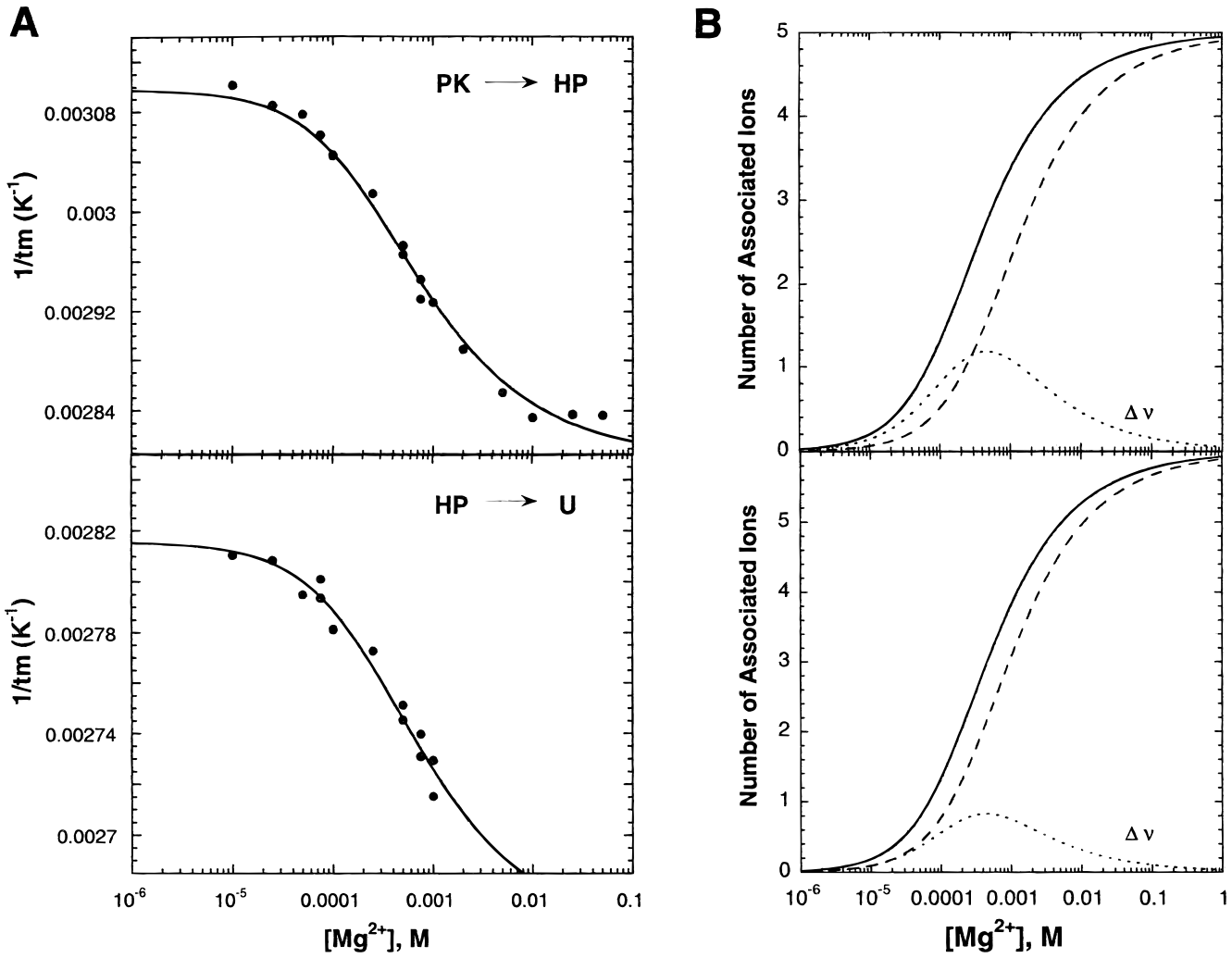

FIGURE 4. **A**: Effect of [Mg^{2+}] on the t_m for the two unfolding transitions in the wild-type MMTV vpk pseudoknot in the presence of 50 mM KCl. The dependence of $1/t_m$ on [Mg^{2+}] for the first transition (PK $\rightarrow$ HP) is shown at the top and for the second transition (HP $\rightarrow$ U) at the bottom. The continuous line represents the fit of the experimental data to a nonspecific binding model (Nixon & Giedroc, 1998). **B**: Calculated binding isotherms for the folded (ν_f: solid line) and unfolded (ν_u: dashed line) forms and the difference ($\Delta\nu$: dotted line) between them.

TABLE 2. Mg^{2+} affinities [K_i, (M^{-1})] and number of ions released upon unfolding for the MMTV pseudoknots.[a]

	Transition 1 pseudoknot → hairpin			Transition 2 hairpin → unfolded		
RNA	K_f	K_u	$\Delta\nu$[b]	K_f	K_u	$\Delta\nu$[b]
MMTV	2,100 (±150)	600 (±50)	1.12	1,600 (±300)	800 (±200)	0.78
U13C	3,500 (±350)	800 (±150)	1.36	1,700 (±300)	900 (±200)	0.74
U13CΔA14	2,600 (±300)	500 (±100)	1.29	1,400 (±300)	700 (±200)	0.77
MMTV $(Co(NH_3)_6)^{3+}$	73,400 (±6,800)	12,000 (±1,600)	1.42	—	—	—

[a]Determined from analysis of UV melting profiles at 50 mM KCl. *m*, the number of potential binding sites, was fixed at 10 and 12 for the first and second unfolding transitions, respectively (Laing & Draper, 1994; Nixon et al., 1999).
[b]Values for $\Delta\nu$ are calculated at 10 μM for $(Co(NH_3)_6)^{3+}$ and 0.25 mM for Mg^{2+}.

50 mM KCl compared to the magnitudes of K_f and K_u values determined previously at this and other monovalent salt concentrations (Nixon & Giedroc, 1998; Nixon et al., 1999; Theimer & Giedroc, 1999). These data suggest that it is unlikely that the A14 deletion causes the loss of a specific ion binding site or results in differential accumulation of ions in the pseudoknot.

Recently, a localized $Co(NH_3)_6^{3+}$ or Mg^{2+} ion in the MMTV vpk pseudoknot was identified and characterized structurally by NMR (Gonzalez & Tinoco, 1999). This metal-binding site was found in the major groove of stem 2 where close approach of the phosphate backbone of loop 1 causes a region high in negative electrostatic potential that would be predicted to be lost when unfolding of stem 1 moves the backbone of loop 1 out of the major groove. A weakly localized cobalt (III) hexaammine ion was predicted to occur in the autoregulatory RNA pseudoknots from bacteriophage T2 and T4 *gene 32* mRNA from imino proton perturbation NMR spectroscopy (Nixon et al., 1999). In light of these recent studies, the average affinity and stoichiometry of those $Co(NH_3)_6^{3+}$ ions linked to the stability of the folded pseudoknot over the partially folded molecule was determined by analyzing the effects of $Co(NH_3)_6^{3+}$ (5 μM–5 mM) in a background of 50 mM KCl on the unfolding of the MMTV pseudoknot. For the pseudoknot-to-hairpin unfolding transition, the $Co(NH_3)_6^{3+}$ binding affinities for the folded (K_f) and unfolded (K_u) forms were found to be 73,400 (±6,800) M^{-1} and 12,000 (±1,600) M^{-1}, respectively, using a +3 binding site model (Nixon et al., 1999). These values are in excellent agreement with affinities calculated for pseudoknot-to-hairpin transitions involving weakly localized $Co(NH_3)_6^{3+}$ binding under similar solution conditions (Nixon et al., 1999). A net release of ≈1.4 ions occurs in the first unfolding step of the MMTV RNA and, from studies of similar hairpins, there is likely to be an additional net release of ≈1 ion from the hairpin-to-unfolded transition (Nixon et al., 1999). The net number of trivalent ions released upon unfolding of the pseudoknot is largely consistent with the solution structure of the MMTV pseudoknot-$Co(NH_3)_6^{3+}$ complex as well as the number of ions predicted to interact with this pseudoknot from Brownian dynamics simulations (Hermann & Westhof, 1998; Gonzalez & Tinoco, 1999). Thus, it is tempting to conclude that this ion localized in the major groove of stem 2 plays a major role in stabilizing the pseudoknotted conformation against thermal denaturation. Similar findings characterize the effects of $Co(NH_3)_6^{3+}$ on the unfolding of the T2 gene *32* autoregulatory pseudoknot (Nixon et al., 1999).

Effects of monovalent ions on the stability of the MMTV pseudoknots

Restrained molecular dynamics simulations of the solution structure of the MMTV vpk pseudoknot carried out in the presence of explicit water molecules and Na^+ ions suggest that several Na^+ ions are coordinated by the molecule, some interacting directly with A14, and that coordination of Na^+ ions adds significant stabilization to the molecule by allowing loop 2 to stack close to the minor groove of stem 1 (Le et al., 1998). The high-resolution crystal structure of the frameshifting pseudoknot from beet western yellows virus (BWYV) has several interesting structural features, including a Na^+ ion proposed to be specifically coordinated in the minor groove that is thought to stabilize loop 2–stem 1 interactions (Su et al., 1999). In neither case has the specificity of these monovalent ion–RNA interactions been directly probed, nor has their specific role, if any, in stabilizing the RNA. To determine if the MMTV vpk pseudoknot exhibits specific monovalent binding that is directly linked to the stability of the wild-type RNA relative to the ΔA14 mutant, the unfolding of all three MMTV-derived pseudoknots was examined in the presence of varying concentrations of group 1A monovalent chloride salts (LiCl, KCl, NaCl, CsCl, RbCl) and NH_4Cl up to 1 M.

Representative optical melting profiles of the U13C RNA in the presence of 100 mM CsCl or 100 mM LiCl are shown in Figure 5A with the dependence of t_m on the ionic radius of the monovalent cation at 100 mM MCl shown in Figure 5B. Three points can be made from these data. First, the trend in the stabilizing effects of monovalent ions is identical for the PK → HP and HP → U unfolding transitions with the smallest monovalent ion, Li^+, maximally stabilizing and comparable

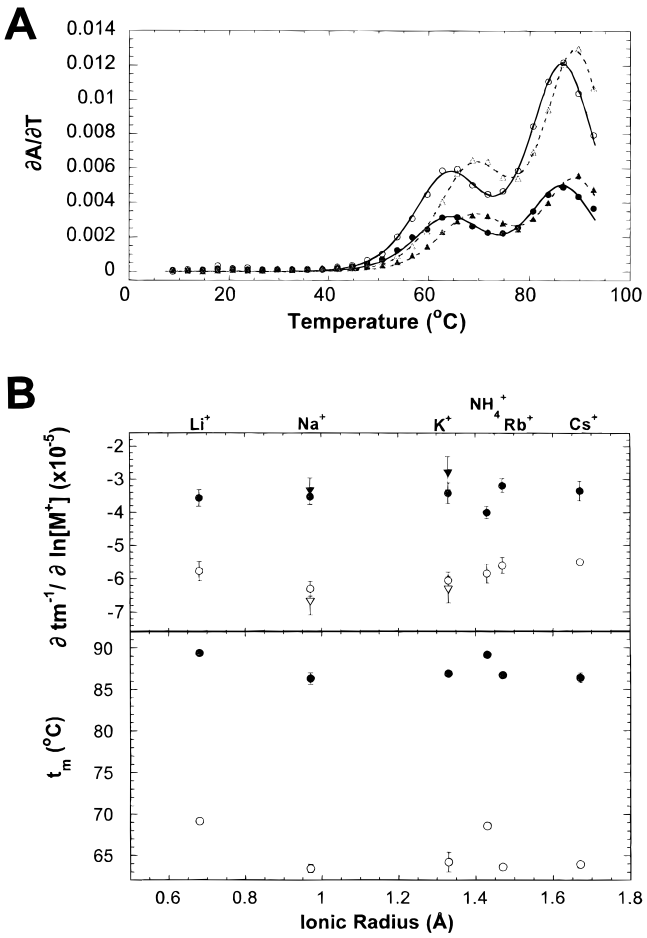

FIGURE 5. Salt dependence of t_m for the U13C pseudoknot. **A**: Optical melting profiles for U13C in the presence of 100 mM LiCl (circles) and 100 mM CsCl (triangles). Optical data is represented by filled and open symbols corresponding to ∂A/∂T monitored at 260 and 280 nm, respectively with the fits to the data represented as solid and dashed lines for CsCl and LiCl, respectively. **B** (upper): Slope of t_m^{-1} versus ln[MCl] plot as a function of ionic radius for transition 1 (○,▽) and transition 2 (●,▼) for U13C and U13CΔA14, respectively. From $\partial t_m^{-1}/\partial \ln[M^+] = -\Delta nR/\Delta H$ (Record & Lohman, 1978), the average $\partial t_m^{-1}/\partial \ln[M^+]$ and Δn are $-5.9 (\pm 0.3) \times 10^{-5}$ and 1.5 ± 0.1, and $-3.5 \pm 0.3) \times 10^{-5}$ and 1.1 ± 0.1 for transitions 1 and 2, respectively. **B** (lower): Dependence of t_m on the ionic radius of the monovalent cation for transition 1 (○) and transition 2 (●) of U13C at 100 mM MCl.

to that of NH_4^+ ion, and the larger ion, Cs^+, least effective. Although the trend is the same, the relative ability of Li^+ versus Cs^+ to stabilize the pseudoknot unfolding transition relative to the hairpin unfolding transition is modestly larger. For example, Li^+ and NH_4^+ ions stabilize the RNA more than do larger group 1A monovalent ions with an ≈5–8 °C difference in t_m between Li^+ and Cs^+ for the pseudoknot-to-hairpin unfolding transition and an ≈2–4 °C difference for the hairpin-to-unfolded transition. Second, the behavior observed at 100 mM monovalent salt for the U13C RNA is observed at all other monovalent salt concentrations from 50 mM to 1 M, as the $\partial t_m^{-1}/\partial \ln[M^+]$ values are essentially independent of M^+ (Fig. 5B). Furthermore, $\partial t_m^{-1}/\partial \ln[M^+]$ averaged over all monovalent ion types for the PK → HP transition is consistently larger than that observed for the HP → U transition. Application of a simple polyelectrolyte model to the monovalent ion concentration dependence of these unfolding transitions suggests that 1.5 ± 0.1 and 1.1 ± 0.1 ions are released upon unfolding of the pseudoknot and hairpin intermediate, respectively. Third, the $\partial t_m^{-1}/\partial \ln[M^+]$ where M^+ is Na^+ and K^+ are identical for the U13C and U13CΔA14 RNAs (Fig. 5B).

The observed preferential stabilization by smaller monovalent ions and NH_4^+ ion is identical to that observed previously for another RNA pseudoknot (Gluick et al., 1997). In that study, it was suggested that size-based monovalent ion selectivity may be a common feature of the high charge densities created by RNA tertiary structures where the competing effects of "small cavity size," which would favor smaller ions, and relative ease of dehydration, which would favor larger ions relative to Li^+ and NH_4^+, may be largely offsetting. Our findings with mono-, di-, and trivalent ions are largely consistent with delocalized or weakly localized ions that provide substantial stability to these RNAs. These experiments also reveal that the MMTV-derived RNAs are stabilized to similar extents by mono- and multivalent ions and exhibit similar monovalent ion specificity profiles. This would seem to rule out highly specific structure-inducing interactions with a dehydrated Na^+ ion that involve A14 like those observed in a recent molecular dynamics simulation (Le et al., 1998). Consistent with this, no evidence for a highly ordered and tightly packed loop 2 was observed in the recent refinement of the MMTV-vpk pseudoknot NMR structure (Gonzalez & Tinoco, 1999).

Free energy increment due to A14 and a comparison of ΔG° with $\Delta G°_{predicted}$

Optical and calorimetric melting profiles in the presence of 1 M NaCl are shown in Figure 6 with thermodynamic parameters compiled in Table 1. All three RNAs are significantly more stable at 1 M NaCl with an average increase in t_m and enthalpy of 20 °C and 8 kcal mol^{-1} for the first transition and 10 °C and 3 kcal mol^{-1} for the second transition, giving a total stabilization of 5.5–6.5 kcal mol^{-1} in free energy at 37 °C compared to 50 mM KCl.

The contribution that the unpaired adenosine makes to the global stability ($\Delta G°_{37}$) of the molecule can be obtained by calculating $\Delta\Delta G°_{37}$ between the U13C and U13CΔA14 RNAs (Table 1). Simple inspection of the melting profiles reveals that the contribution is clearly small relative to the total $\Delta G°_{37}$ for the molecule (≈18 kcal mol^{-1}). However, it is $\Delta\Delta G°_{37}$ for the first unfolding transition (PK → HP) that directly measures the stability increment for the unpaired adenosine on the pseudoknot formation. Considering all of the optical and DSC

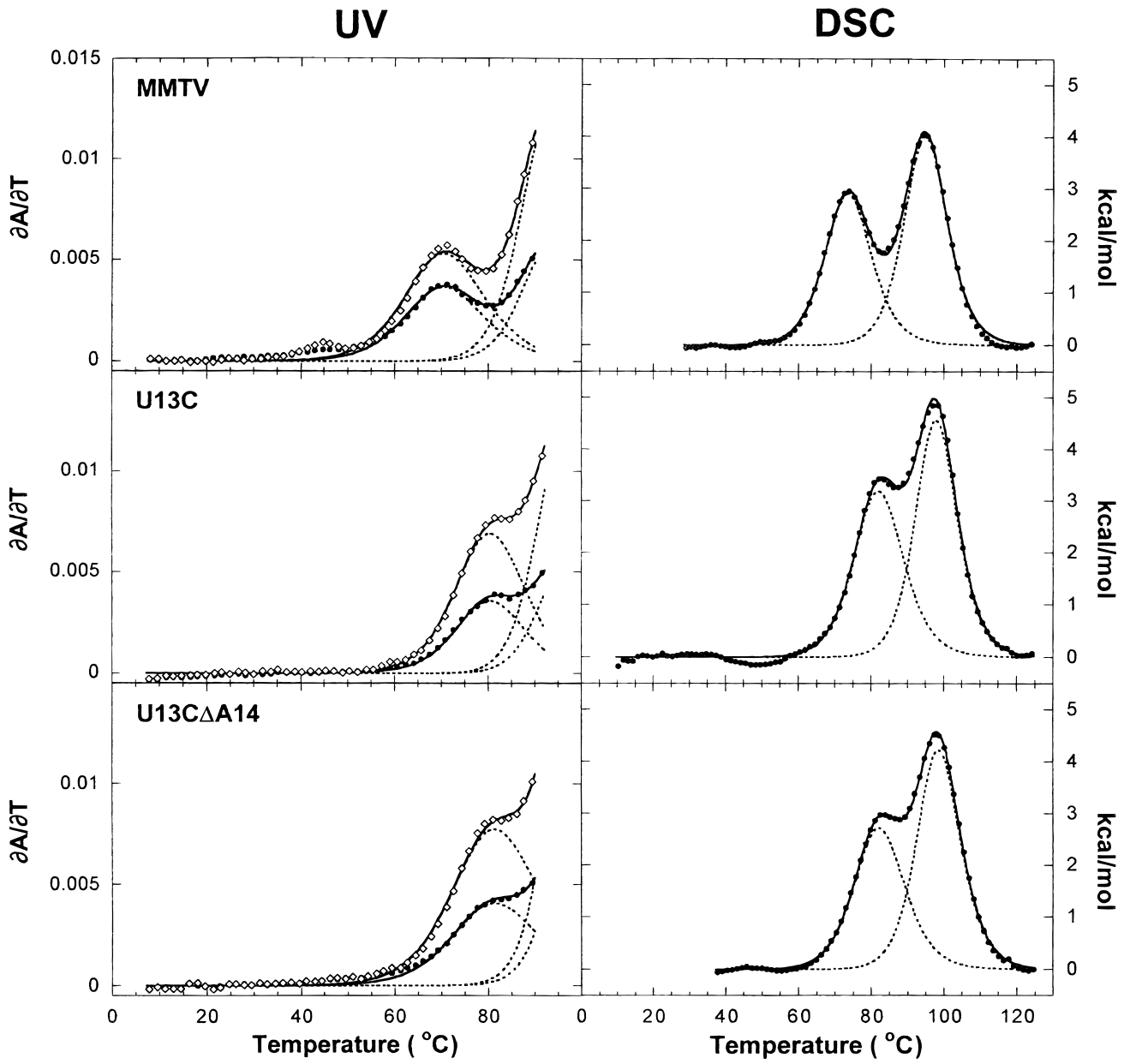

FIGURE 6. Optical and calorimetric melting profiles for the MMTV pseudoknots in the presence of 1 M NaCl. Optical melting profiles are shown on the left, with DSC profiles shown on the right. The composite fit (solid line) is superimposed on the calorimetry data (•). Optical data is represented by black (•) and gray-scale (◇) corresponding to ∂A/∂T monitored at 260 and 280 nm, respectively, with the fits represented as solid lines. Individual transitions are represented by dashed lines.

data collected over a wide range of salt concentrations and types reveals that $\Delta\Delta G^{\circ}_{37}$ is 0.7 ± 0.2 kcal mol^{-1} under weakly stabilizing conditions (low monovalent and low magnesium concentrations) and 1.4 ± 0.2 kcal mol^{-1} under strongly stabilizing conditions (0.5–1 M monovalent salt). This value compares to −0.7 ± 0.7 kcal mol^{-1} for the HP → U transition that does not vary consistently with solution conditions. $\Delta\Delta G^{\circ}_{37}$ for the effect of deletion of A14 on the PK → HP transition is similar in magnitude to the $\Delta\Delta G^{\circ}_{37}$ (0.5–1.0 kcal mol^{-1}) that results from deletion of the putative intercalated A15 in the mIAP *gag-pro* frameshifting pseudoknot (Theimer & Giedroc, 1999). Although the stability increment due to A14 is clearly small, it is important to point out that the net enthalpy gain that results when A14 becomes wedged between the two helical stems ($\Delta\Delta H$ = 6.6 ± 2.1 kcal mol^{-1}) is sufficient to offset a potentially large entropic penalty (upwards of 3.2 kcal mol^{-1}) for creating what is effectively a single nucleotide bulge loop within the context of a helical stem (Fig. 1). This small, favorable free energy increment due to A14 contrasts sharply with the thermodynamic behavior of a single, unpaired adenosine within stem 2 in the mIAP *gag-pro* pseudoknot, which exhibits properties expected

for an extrahelical, unpaired nucleotide (Theimer & Giedroc, 1999).

Predictions from the nearest neighbor model reveal that 3′ stacking of A14 on stem 2 and 5′ stacking of the same base on stem 1 would be predicted to contribute $\Delta G^\circ_{37} \approx 1.3$–$1.9$ kcal mol^{-1} to the stability at 1 M Na^+. This is consistent with the experimentally determined value of 1.4 ± 0.2 kcal mol^{-1}, which argues that any entropic loop penalty for intercalation of A14 is small. If the unpaired adenosine merely disrupts the C-G/G-C coaxial stacking interaction ($\Delta G^\circ_{37} \approx 3.0$ kcal mol^{-1}), the ΔA14 mutation would be expected to be *stabilizing*, which is not the case; nor is this the case in the mIAP pseudoknot (Theimer & Giedroc, 1999).

In a recent survey of crystallographic and solution structures, Burkard et al. (1999) observe a correlation between 3′ unpaired nucleotides that are stacked in RNA structures with the thermodynamic stability of the stack in the context of short helices. They observe that in 83% of 3′ unpaired bases with $-\Delta G^\circ_{37}$ (stack) > 0.7 kcal mol^{-1}, and 100% of the cases where a 3′ A or G is stacked on a closing G-C base pair ($-\Delta G^\circ_{37}$ (stack) $=$ 1.7 kcal mol^{-1}), a stacked nucleotide is observed in the structure. This 3′ stacking interaction is identical to that observed for the wedged adenosine at the helical junctions of the mIAP, SRV-1, FIV, and U13C frameshifting pseudoknots. Deletion of the junction adenosine in mIAP (ΔA15) and U13C (U13CΔA14) gives rise to a destabilization similar in magnitude to the 3′ unpaired nucleotide stacking interaction (Theimer & Giedroc, 1999). Therefore, a good approximation to use in secondary structure prediction of pseudoknots may be that an unpaired nucleotide at the helical junction will be stacked on stem 2 between the helical stems if the stack is worth $\geq$0.7 kcal mol^{-1} in stability and that this interaction is worth 1.4 kcal mol^{-1} in free energy. Although this does not preclude pseudoknots that can potentially form an A-U base pair at the helical junction from forming that base pair, for example, FIV or SRV-1, it suggests that, in both cases, the adenosine is more likely to be stacked on stem 2 than be extrahelical.

The experimentally determined free energies at 1 M NaCl can also be compared to predictions from the modified INN-HB Turner rules (Xia et al., 1998) directly if a pseudoknot loop penalty (Gultyaev et al., 1999) is applied to those predictions. Using a value of 10.6 kcal mol^{-1} for the pseudoknot loop closing entropic penalties for all three molecules (Gultyaev et al., 1999), the predicted ΔG°_{37} values for MMTV, U13C, and U13CΔA14 become 15.8, 17.4, and 17.4 kcal mol^{-1}, respectively. These values are in agreement with the experimental values of 15.7, 18.8, and 17.3 kcal mol^{-1}, respectively. Strikingly, the difference between the experimental and predicted ΔG°_{37} for U13C (1.4 kcal mol^{-1}) is identical to the experimental value of $\Delta\Delta G^\circ_{37}$ for U13C versus U13CΔA14 pseudoknots. However, the same does not hold for the MMTV vpk pseudoknots as would be expected. In any case, the good agreement between theoretical and predicted stabilities using these loop closing penalties may make it easier to identify and quantitate unusual stabilizing interactions outside of Watson–Crick base-pairing and entropically dominated loop-closing penalties in H-type pseudoknots.

CONCLUSIONS

Precisely how RNA pseudoknots positioned downstream of a slippery site stimulate −1 ribosomal frameshifting is currently unknown, but may involve features of a particular structure, and/or tertiary folds of an appropriate stability. Structure-probing and NMR data currently available for pseudoknots derived from retroviruses, coronaviruses, and luteoviruses, however, suggest that there may well be more than one structural motif that can stimulate ribosomal frameshifting (Shen & Tinoco, 1995; Alam et al., 1999; Napthine et al., 1999). However, with respect to MMTV and closely related viruses, a bent conformation facilitated by the wedged adenosine appears to be a primary determinant for frameshifting (Chen et al., 1995, 1996; Shen & Tinoco, 1995; Sung & Kang, 1998).

The work presented here shows that pseudoknots that strongly stimulate frameshifting, MMTV vpk and U13C RNAs, and a coaxially stacked RNA that shows little stimulation of frameshifting, U13CΔA14, all form pseudoknots of very similar global stabilities and mono-, di-, and multivalent ion-binding properties. We could find no evidence for differential accumulation of monovalent or divalent ions in the coaxially stacked versus bent pseudoknots or for significant stabilizing interactions in loop 2 that are dependent on specific coordination of monovalent ions in the context of wedged versus ΔA14 pseudoknots. All RNAs studied here appear to unfold via the same hairpin intermediate, which is separated in free energy from the pseudoknot by relatively similar extents in all three cases, with the wedged and ΔA14 pseudoknots differing from each other by 1.4 kcal mol^{-1} at 1 M Na^+. Although it is unknown to what extent such a difference in stabilization might alter the population distribution of RNA structures (folded and unfolded) at the ribosome, it seems unlikely that frameshifting efficiency will be strongly correlated with the global stability of the RNAs. This is consistent with previous findings that show that insertion of an RNA hairpin of a stability equal to or greater than that predicted for the pseudoknot is far less effective at stimulating frameshifting than is the pseudoknot itself (Brierley et al., 1991; ten Dam et al., 1995).

Apart from global structure and stability, another feature that might be exploited by the ribosome is the *rate* at which the fully folded and partially folded conformers can interconvert. It may be possible that insertion of a wedged nucleotide and/or the presence of other stabilizing interactions at or near the helical junction are

particularly poised to alter the rate of pseudoknot unfolding, even in the absence of relatively small differences in global stability. Certainly, recent work derived from analyzing the effects of loop 2–stem 1 compensatory mutations on frameshifting efficiency of MMTV-IBV chimeric pseudoknots supports the presence of defined, though not yet structurally characterized, interactions between the 3′ nucleotide in loop 2 (an adenosine) and the base of stem 1 nearest the helical junction, which are functionally important in some contexts (Liphardt et al., 1999). The extent to which these interactions contribute to the stability is unknown, but it is likely to be small compared to the global stability of the RNA if our work on the mIAP (Theimer & Giedroc, 1999) and MMTV pseudoknots (this work) is generalizable to other *gag-pro* frameshifters. It may be that these interactions provide a topological constraint to pseudoknot unwinding or otherwise subtly alter the junction flexibility in such a way that is compatible with function.

A major finding is that we have quantified the thermodynamic effects of the deletion of an unpaired adenosine nucleotide on the stability of an H-type RNA pseudoknot involved in ribosomal frameshifting. We find that this deletion is modestly destabilizing by 1.4 kcal mol^{-1}. This unpaired adenosine provides a stabilizing free energy increment similar in magnitude to that of an 3′ unpaired nucleotide stacked on a closing base pair at a helical terminus. Knowledge of this free energy increment may further enable prediction of RNA secondary structure from nucleotide sequence.

MATERIALS AND METHODS

RNA synthesis and purification

RNAs with the sequences shown in Figure 1 were prepared by in vitro transcription using T7 RNA polymerase and partially double-stranded templates as described previously (Du et al. 1996; Qiu et al. 1996). Crude RNAs were purified by denaturing PAGE, visualized by UV shadowing and electroeluted using an S&S electroeluter. The recovered RNA was loaded onto a C18-cartridge (Alltech), eluted with a 50% methanol wash, taken to dryness, and subjected to exhaustive dialysis against 10 mM MOPS, pH 7.0, 50 mM KCl. The first change of dialysis buffer contained 10 mM EDTA, with the subsequent (2–3) changes containing no EDTA. RNAs were stored at −20 °C until use. Samples were prepared for thermal denaturation by diluting into final dialysis buffer, adding the appropriate concentration of $MgSO_4$, heating at 65 °C for 10 min, and slow cooling to room temperature.

Thermal denaturation experiments

All optically monitored RNA thermal denaturation experiments were collected on a temperature-controller equipped Cary 1 spectrophotometer operating in double-beam mode. All melts were collected in 10 mM MOPS, pH 7.0, and 50 mM KCl with the indicated concentration of $MgSO_4$. Capped cells were used and percent transmittance was recorded as a function of temperature at both 260 and 280 nm simultaneously. Samples were loaded into room temperature cuvettes and the cells allowed to equilibrate at 5 °C for 30 min. The temperature controller was ramped at a rate of 0.3 °C/min from 5–100 °C. Data points were collected every 0.3–0.4 °C as determined by a temperature probe inserted into a cuvette containing final dialysis buffer.

Analysis of UV thermal melting profiles

Cary 1 report files were converted from percent transmittance to absorbance and subjected to piece-wise linear interpolation. The interpolated sets of data were then smoothed over a 4 °C window and the melting profile was generated by taking the first derivative of absorbance with respect to temperature ($\partial A/\partial T$) and plotted as a function of temperature. Melting profiles were subjected to nonlinear least squares parameter estimation of $t_{m,i}$, ΔH_i, and A_i, for each ith sequential unfolding transition via application of an unfolding model involving interacting sequential two-state unfolding transitions (Laing & Draper, 1994) using the t-melt program running on an SGI O_2 unix workstation as described previously (Nixon & Giedroc, 1998; Theimer et al., 1998; Theimer & Giedroc, 1999). The van't Hoff analysis of the UV melting data assumes that ΔCp° is zero, which is a reasonable approximation given the observed agreement between thermodynamic parameters derived from optical and calorimetric data.

Calorimetry experiments

All calorimetry scans were collected on a Microcal VP-DSC. RNA concentrations in the sample cell varied between 30–50 μM in a 0.5-mL cell. Samples for differential scanning calorimetry at 10 mM MOPS, pH 7.0, 50 mM KCl with 0 mM Mg^{2+} or 1 M NaCl were made by dialyzing overnight against the appropriate buffer, with the dialysis buffer used in the reference chamber. DSC samples at 0.5 mM Mg^{2+} were made by adding the appropriate concentration of Mg^{2+} to the equilibrated 0 mM Mg^{2+} sample and buffer. Samples were heated at 65 °C for 10 min, slow cooled to room temperature, and degassed. Samples were then loaded into room temperature cells, cooled to 1 °C, and allowed to equilibrate for 30 min. The temperature was ramped at a rate of 1 °C/min from 1–120 °C. Baseline scans were run under identical conditions using final dialysis buffer in both the sample and reference cells.

Analysis of differential scanning calorimetry data

VP-DSC data files were analyzed using the program Origin from Microcal. The collected buffer baseline scan was subtracted from the RNA sample scan and the data corrected for the concentration of RNA in the cell. The data were analyzed using three different sequential unfolding models. For the two-state and non-two-state models the data were subjected to a cubic baseline correction, and the calorimetric enthalpy,

H_{cal}, calculated from the area under the baseline-corrected curve before either fit is applied. In the two-state model, van't Hoff enthalpies and melting temperatures were determined utilizing a sequential two-state unfolding model fit minimized to represent the experimental data and also to minimize the difference between the sum of the van't Hoff enthalpies and the total calorimetric enthalpy. In the non-two-state model, van't Hoff enthalpies, calorimetric enthalpies and melting temperatures for each transition were determined utilizing a sequential two-state unfolding model fit that did not require that the van't Hoff enthalpy equal the calorimetric enthalpy for each transition as defined by the area under the curve. In the third model, which is a sequential two-state unfolding model including a nonzero ΔCp°, the data are not subjected to a preliminary baseline correction, the total H_{cal} is not calculated, and the fit includes a ΔCp° term for each transition and a fit to pre- and posttransition baselines. Because all three models fit the data equivalently well and returned essentially identical van't Hoff parameters for ΔH and t_m, the simple two-state model was used.

The sequential unfolding model used for fitting the calorimetry data is identical to that used for the optical data with the equilibrium constants, the partition function, and the sum of the terms in which an individual transition participates, described in the same way (Theimer & Giedroc, 1999). Instead of an absorbance change, the signal observed is a change in the total molar heat content of the system, which is a function of the molar enthalpy changes for each individual transition (Theimer & Giedroc, 1999).

ACKNOWLEDGMENTS

This work was supported by National Institutes of Health (NIH) grant AI40187 to D.P.G. and D.W. Hoffman. The Microcal VP-DSC was supported in part by grants from the Texas Agricultural Experiment Station and NIH grant GM42569 to D.P.G. We thank Dr. Jon A. Christopher for the program t-melt (Theimer et al., 1998) and we also thank Mr. Brian Cannon for highly purified T7 RNA polymerase (supported by the Howard Hughes Medical Institute Undergraduate Biological Sciences Education Program Grant 7119571195-539101).

Received September 15, 1999; returned for revision October 20, 1999; revised manuscript received December 14, 1999

REFERENCES

Alam SL, Wills NM, Ingram JA, Atkins JF, Gesteland RF. 1999. Structural studies of the RNA pseudoknot required for readthrough of the *gag*-termination codon of murine leukemia virus. *J Mol Biol 288*:837–852.

Atkins JF, Gesteland RF. 1999. Intricacies of ribosomal frameshifting. *Nature Struct Biol 288*(5):837–852.

Brierley I, Rolley NJ, Jenner AJ, Inglis SC. 1991. Mutational analysis of the RNA pseudoknot component of a coronavirus ribosomal frameshifting signal. *J Mol Biol 220*:889–902.

Burkard ME, Kierzek R, Turner DH. 1999. Thermodynamics of unpaired terminal nucleotides on short RNA helixes correlates with stacking at helix termini in larger RNAs. *J Mol Biol 290*:967–982.

Chamorro M, Parkin N, Varmus HE. 1992. An RNA pseudoknot and an optimal heptameric shift site are required for highly efficient ribosomal frameshifting on a retroviral messenger RNA. *Proc Natl Acad Sci USA 89*:713–717.

Chen X, Chamorro M, Lee SI, Shen LX, Hines JV, Tinoco I Jr, Varmus HE. 1995. Structural and functional studies of retroviral RNA pseudoknots involved in ribosomal frameshifting: Nucleotides at the junction of the two stems are important for efficient ribosomal frameshifting. *EMBO J 14*:842–852.

Chen X, Kang H, Shen LX, Chamorro M, Varmus HE, Tinoco I Jr. 1996. A characteristic bent conformation of RNA pseudoknots promotes −1 frameshifting during translation of retroviral RNA. *J Mol Biol 260*:479–483.

Du Z, Giedroc DP, Hoffman DW. 1996. Structure of the autoregulatory pseudoknot within the gene *32* messenger RNA of bacteriophages T2 and T6: A model for a possible family of structurally related RNA pseudoknots. *Biochemistry 35*:4187–4198.

Du Z, Hoffman DW. 1997. An NMR and mutational study of the pseudoknot within the gene 32 mRNA of bacteriophage T2: Insights into a family of structurally related RNA pseudoknots. *Nucleic Acids Res 25*:1120–1135.

Du Z, Holland JA, Hansen MR, Giedroc DP, Hoffman DW. 1997. Base pairings within the RNA pseudoknot associated with the Simian retrovirus-1 *gag-pro* frameshift site. *J Mol Biol 270*:464–470.

Fresco JR, Klotz LC, Richards EG. 1963. A new spectroscopic approach to the determination of helical secondary structure in ribonucleic acids. *Cold Spring Harbor Symp Quant Biol 28*:83–90.

Gluick TC, Wills NM, Gesteland RF, Draper DE. 1997. Folding of an mRNA pseudoknot required for stop codon readthrough: Effects of mono- and divalent ions on stability. *Biochemistry 36*:16173–16186.

Gonzalez RL Jr, Tinoco I Jr. 1999. Solution structure and thermodynamics of a divalent metal ion binding site in an RNA pseudoknot. *J Mol Biol 289*:1267–1282.

Gultyaev AP, van Batenberg FHD, Pleij CWA. 1999. An approximation of loop free energy values of RNA H-pseudoknots. *RNA 5*:609–617.

Hermann T, Westhof E. 1998. Exploration of metal ion binding sites in RNA folds by Brownian-dynamics simulations. *Structure 6*: 1303–1314.

Holland JA, Hansen MR, Du Z, Hoffman DW. 1999. An examination of coaxial stacking of helical stems in a pseudoknot motif: The gene *32* messenger RNA pseudoknot of bacteriophage T2. *RNA 5*:257–271.

Kang H, Hines JV, Tinoco I Jr. 1996. Conformation of a nonframeshifting RNA pseudoknot from mouse mammary tumor virus. *J Mol Biol 259*:135–147.

Kang H, Tinoco I Jr. 1997. A mutant RNA pseudoknot that promotes ribosomal frameshifting in mouse mammary tumor virus. *Nucleic Acids Res 25*:1943–1949.

Laing LG, Draper DE. 1994. Thermodynamics of RNA folding in a conserved ribosomal RNA domain. *J Mol Biol 237*:560–576.

Laing LG, Gluick TC, Draper DE. 1994. Stabilization of RNA structure by Mg ions. Specific and nonspecific effects. *J Mol Biol 237*:577–587.

Le SY, Chen JH, Pattabiraman N, Maizel JV. 1998. Ion–RNA interactions in the RNA pseudoknot of a ribosomal frameshifting site—molecular modeling studies. *J Biomol Struct Dyn 16*:1–11.

Liphardt J, Napthine S, Kontos H, Brierly I. 1999. Evidence for an RNA pseudoknot loop–helix interaction essential for efficient −1 ribosomal frameshifting. *J Mol Biol 288*:321–335.

Mathews DH, Sabina J, Zuker M, Turner DH. 1999. Expanded sequence dependence of thermodynamic parameters improves prediction of RNA secondary structure. *J Mol Biol 288*:911–940.

Morikawa S, Bishop DHL. 1992. Identification and analysis of the *gag-pol* ribosomal frameshift site of feline immunodeficiency virus. *Virology 186*:389–397.

Napthine S, Liphardt J, Bloys A, Routledge S, Brierly I. 1999. The role of RNA pseudoknot stem 1 length in the promotion of efficient −1 ribosomal frameshifting. *J Mol Biol 288*:305–320.

Nixon PL, Giedroc DP. 1998. Equilibrium unfolding (folding) pathway of a model H-type pseudoknotted RNA: The role of magnesium ions in stability. *Biochemistry 37*:16116–16129.

Nixon PL, Giedroc DP. 2000. Energetics of a strongly pH dependent RNA tertiary structure in a frameshifting pseudoknot. *J Mol Biol 296*:659–671.

Nixon PL, Theimer CA, Giedroc DP. 1999. Thermodynamics of stabilization of RNA pseudoknots by Cobalt(III) Hexaammine. *Biopolymers 50*:443–458.

Puglisi JD, Wyatt JR, Tinoco I Jr. 1990. Conformation of an RNA pseudoknot. *J Mol Biol 214*:437–453.

Qiu H, Kaluarachchi K, Du Z, Hoffman DW, Giedroc DP. 1996. Thermodynamics of folding of the RNA pseudoknot of the T4 gene *32* autoregulatory messenger RNA. *Biochemistry 35*:4176–4186.

Record MT Jr, Lohman TM. 1978. A semiempirical extension of polyelectrolyte theory to the treatment of oligoelectrolytes: Application to oligonucleotide helix-coil transitions. *Biopolymers 17*:159–166.

Shen LX, Tinoco I Jr. 1995. The structure of an RNA pseudoknot that causes efficient frameshifting in mouse mammary tumor virus. *J Mol Biol 247*:963–978.

Strobel SA, Doudna JA. 1997. RNA seeing double—close packing of helices in RNA tertiary structure. *Trends Biochem Sci 22*:262–266.

Su L, Chen L, Egli M, Berger JM, Rich A. 1999. Minor groove RNA triplex in the crystal structure of a ribosomal frameshifting viral pseudoknot. *Nature Struct Biol 6*:285–292.

Sung D, Kang H. 1998. Mutational analysis of the RNA pseudoknot involved in efficient ribosomal frameshifting in simian retrovirus-1. *Nucleic Acids Res 26*:1369–1372.

ten Dam EB, Verlaan PWG, Pleij CWA. 1995. Analysis of the role of the pseudoknot component in the SRV-1 *gag-pro* ribosomal frameshift signal: Loop lengths and stability of the stem regions. *RNA 1*:146–154.

Theimer CA, Giedroc DP. 1999. Equilibrium unfolding pathway of an H-type RNA pseudoknot which promotes programmed −1 ribosomal frameshifting. *J Mol Biol 289*:1283–1299.

Theimer CA, Wang Y, Hoffman DW, Krisch HM, Giedroc DP. 1998. Non-nearest neighbor effects on the thermodynamics of unfolding of a model mRNA pseudoknot. *J Mol Biol 279*:545–564.

Turner DH, Sugimoto N, Freier SM. 1988. RNA structure prediction. *Annu Rev Biophys Biophys Chem 17*:167–192.

Wyatt JR, Puglisi JD, Tinoco I Jr. 1990. RNA pseodoknots. Stability and loop size requirements *J Mol Biol 214*:455–470.

Xia T, SantaLucia J Jr, Burkard ME, Kierzek R, Shroeder SJ, Jiao X, Cox C, Turner DH. 1998. Thermodynamic parameters for an expanded nearest-neighbor model for formation of RNA duplexes with Watson–Crick base pairs. *Biochemistry 17*:14719–14735.